Entropy Inflection and Invisible Low-Energy States: Defensive Alliance Examle

Yi-Zhi Xu, Chi Ho Yeung, Hai-Jun Zhou, David Saad

Supplementary Information

S1. SIMULATED ANNEALING (SA)

Here we describe the details of the simulated annealing process. Without loss of generality we assume the input graph G is connected. If instead G is formed by two or even more connected components, each of these connected components can be treated separately. The SA process starts from an initial inverse temperature $\beta = \beta_{init}$, which is quite low (e.g., $\beta_{init} = 10^{-3}$). The occupation configuration $\boldsymbol{c} = (c_1, c_2, \ldots, c_N)$ is initialized to be fully occupied, $c_i = 1$ for all the vertices $i \in G$. Each occupied vertex contributes a unit energy, so the total energy of the initial configuration is $E(\boldsymbol{c}) = N$. At each value of the inverse temperature β the configuration $\boldsymbol{c}$ is allowed to evolve for a time w_0 through a sequence of single-vertex and multiple-vertex state flips, and the mean value of the configuration energies is recorded during this time window w_0. Then the inverse temperature is increased to $\beta \leftarrow \beta + \varepsilon$ with ε being a small value, e.g., $\varepsilon = 0.001$ or $\varepsilon = 0.01$. The SA process continues to run at this and later elevated β values until the final value β_{final} is reached, which is sufficiently high (e.g., $\beta_{\text{final}} = 10$). The latest configuration $\boldsymbol{c}$ is then returned as the output of the SA evolution process. For the regular random (RR) graph instances studied in this work, we have checked that the subgraphs formed by the vertices in these final alliance solutions always have only a single connected component.

We adopt the Metropolis importance-sampling method to update the occupation configurations $\boldsymbol{c}$. In each elementary step of this Markov Chain Monte Carlo evolution dynamics: with probability p_s a single-vertex state flip is attempted, and with the remaining probability $p_m = 1 - p_s$ a multiple-vertex state flip is attempted; and then the evolution time t advances by the incremental change $\delta t = 1/N$ irrespective of whether the proposed change to $\boldsymbol{c}$ was accepted or rejected. One unit time of the SA evolution therefore corresponds to N consecutive flipping trials. Let us emphasize that the SA process generates a stochastic trajectory within the space of strong defensive alliance (SDA) solutions; at any evolution time t the vertex set formed by the occupied vertices of $\boldsymbol{c}$ is always a valid alliance.

We set $p_s = 0.5$ in all our SA simulations. The value of p_m is set to be $p_m = 0.5$ except for the simulation results reported in Fig. S4. The SA algorithm applicable to K-regular graphs is

accessible from the webpage `lib.itp.ac.cn/html/zhouhj/codes.htm`.

A. Single-vertex state flip

A single-vertex flipping trial consists of proposing a state change $c_i \to 1 - c_i$ for a vertex i of the graph, under the constraint that the initial configuration $\boldsymbol{c}$ and the updated configuration $\boldsymbol{c}'$ are both valid alliances. For the initial configuration $\boldsymbol{c}$, let us denote the set of all the flippable vertices from $c_i = 1$ to $c_i = 0$ as $V_{1\to 0}$ and the set of all flippable vertices from $c_j = 0$ to $c_j = 1$ as $V_{0\to 1}$; similarly, for the updated configuration $\boldsymbol{c}'$ the sets of flippable $(1 \to 0)$ and $(0 \to 1)$ vertices are denoted as $V'_{1\to 0}$ and $V'_{0\to 1}$, respectively. The cardinality of a vertex set (say V) is denoted as $|V|$. We conduct single-vertex flipping trials following the rule of importance sampling, which guarantees detailed balance:

1. Generate a uniform real random number r in $[0, 1)$.

2. If $r < \frac{|V_{1\to 0}|}{|V_{1\to 0}|+e^{-\beta}|V_{0\to 1}|}$, randomly choose a flippable occupied vertex i from set $V_{1\to 0}$ and propose a flip from $c_i = 1$ to $c_i = 0$; otherwise randomly choose a flippable empty vertex j from $V_{0\to 1}$ and propose a flip from $c_j = 0$ to $c_j = 1$.

3. Accept this single-vertex flip proposal and the associated new configuration $\boldsymbol{c}'$ with probability $A_s(\boldsymbol{c} \to \boldsymbol{c}')$, whose precise expression being

$$A_s(\boldsymbol{c} \to \boldsymbol{c}') = \min\Big(1,\ \frac{|V_{1\to 0}| + e^{-\beta}|V_{0\to 1}|}{|V'_{1\to 0}| + e^{-\beta}|V'_{0\to 1}|}\Big)\ , \tag{S1}$$

   otherwise keep the old configuration $\boldsymbol{c}$.

B. Multiple-vertex state flip for a regular graph of degree $K = 3$

To better explain the adopted multiple-vertex flipping trials we first consider the special case of a regular graph of degree $K = 3$ (i.e., a 3-regular graph). We define the concepts of empty and occupied bridges as follows: An empty bridge for a 3-regular graph is a path formed by $n \geq 2$ different empty vertices $j_1, j_2, \ldots, j_n$ such that: (1) the whole path is connected to two and only two occupied vertices (called the bridge anchors, e.g., vertices i and m in Fig. S1a) by exactly two edges, attached to the start and end vertices (j_1 and j_n), and there is no other neighboring occupied vertex to the whole path except the two bridge anchors, and (2) there is no other edge between any two vertices of this path except for the $n-1$ edges linking these n empty vertices into

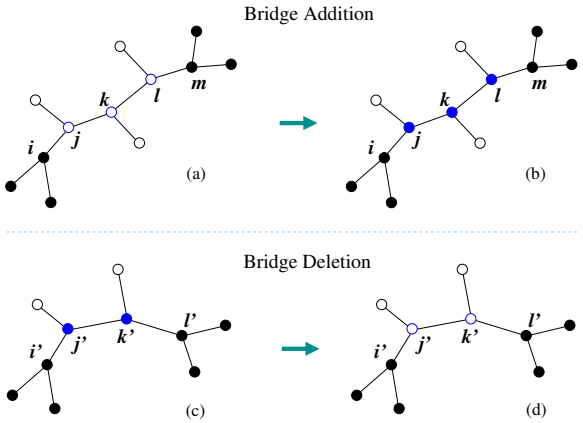

Figure S1: Bridge addition and deletion processes for regular graphs of degree $K = 3$. (a) Vertices i and m serve as the two anchors for an empty bridge (j, k, l) of length $n_1 = 3$ of an occupation configuration $\boldsymbol{c}$. (b) After an empty bridge is flipped to be an occupied bridge, a new configuration $\boldsymbol{c}'$ is formed, and vertices i and m then serve as the two anchors of an occupied bridge (j, k, l) in this new configuration. (c) and (d): An occupied bridge (j', k') of length $n_2 = 2$ anchored to vertices i' and l' is flipped to an empty bridge.

a path. Similarly, an occupied bridge for a 3-regular graph is a path formed by $m \geq 2$ different occupied vertices $k_1, k_2, \ldots, k_m$ such that: (1) all these m vertices have exactly two occupied nearest neighbors, (2) there is no other edge between any two vertices of this path except for the $m-1$ edges linking them into a path, and (3) the start and end vertices (k_1 and k_m) of the bridge are connected to two *different* occupied vertices (the bridge anchors, e.g., vertices i' and l' of Fig. S1c) with each of these two anchors having three occupied nearest neighbors.

For the initial configuration $\boldsymbol{c}$, let us denote by $B_{0\to1}$ the set formed by all the start or end vertices of all the empty bridges, and by $B_{1\to0}$ the set formed by all the start or end vertices of all the occupied bridges. Similarly, the two sets of bridge terminal vertices for the updated configuration $\boldsymbol{c}'$ are denoted as $B'_{0\to1}$ and $B'_{1\to0}$, respectively. Notice that if a vertex $j \in B_{0\to1}$ is flipped to the state $c_j = 1$ all the other vertices of the associated empty bridge must be flipped to be occupied as well; similarly if a vertex $j' \in B_{1\to0}$ is flipped to the state $c_{j'} = 0$ all the other vertices of the associated occupied bridge must be flipped to empty as well (Fig. S1).

To construct an empty bridge of configuration $\boldsymbol{c}$ we proceed as follows: (1) Draw an empty vertex (say j of Fig. S1a) from set $B_{0\to1}$ and regard it as the start of an empty bridge. (2) Then randomly select an empty neighbor (say vertex k) of j and add it to the bridge. (3) Determine whether to stop or to continue: if k has two occupied neighbors, the bridge construction is regarded as a failure and is stopped; otherwise if k has only one occupied neighbor, the bridge construction is regarded as successful and is stopped; otherwise k has no occupied neighbor, then the bridge

is extended by adding an randomly chosen empty neighbor (say vertex l) different from j to the bridge and then step (3) is repeated. If the construction of the empty bridge is successful, the last added vertex (e.g., l in Fig. S1a) must be connected to a single occupied vertex.

The construction of an occupied bridge is slightly simpler: (1) Draw an occupied vertex (say j' of Fig. S1c) from set $B_{1\to 0}$ and regard it as the start of an occupied bridge. (2) Then add a neighboring occupied vertex (say k') with exactly two occupied neighbors to the bridge. (3) Continue this bridge extension process if necessary, until an anchor vertex (say l' in Fig. S1c) is reached. The constructed bridge is regarded as successful if the two anchor vertices i' and l' of the bridge are not identical.

We conduct the multiple-vertex flipping trial from $\boldsymbol{c}$ to $\boldsymbol{c}'$ according to the following rule of importance sampling, which guarantees detailed balance:

1. Generate a uniform real random number r in $[0, 1)$.

2. Perform bridge addition or bridge deletion:

   (2.1). If $r < \frac{|B_{0\to 1}|}{|B_{0\to 1}|+|B_{1\to 0}|}$, then randomly choose an empty vertex j from set $B_{0\to 1}$ and construct an empty path starting from j following the above-mentioned protocol. If the constructed path is not a valid empty bridge, keep the old configuration $\boldsymbol{c}$. If this path is a valid empty bridge, then flip all the vertices in this bridge to be occupied and accept the updated configuration $\boldsymbol{c}'$ with the following probability

   $$A_m^{0\to 1}(\boldsymbol{c}\to\boldsymbol{c}') = \min\left(1,\ \frac{|B_{0\to 1}|+|B_{1\to 0}|}{|B'_{0\to 1}|+|B'_{1\to 0}|} 2^{n_b-1} e^{-\beta n_b}\right), \tag{S2}$$

   where n_b denotes the length of the constructed bridge; otherwise keep the old configuration $\boldsymbol{c}$.

   (2.2). Otherwise $r \geq \frac{|B_{0\to 1}|}{|B_{0\to 1}|+|B_{1\to 0}|}$, then randomly choose an occupied vertex j' from set $B_{1\to 0}$ and extend an occupied path starting from j', following the above-mentioned protocol. If the constructed path is not a valid occupied bridge, keep the old configuration $\boldsymbol{c}$. If this path is a valid occupied bridge, then flip all the vertices in this bridge to be empty and accept the updated configuration $\boldsymbol{c}'$ with the following probability

   $$A_m^{1\to 0}(\boldsymbol{c}\to\boldsymbol{c}') = \min\left(1,\ \frac{|B_{0\to 1}|+|B_{1\to 0}|}{|B'_{0\to 1}|+|B'_{1\to 0}|} 2^{1-n_b} e^{\beta n_b}\right), \tag{S3}$$

   where n_b again denotes the length of the constructed bridge; otherwise keep the old configuration $\boldsymbol{c}$.

C. Multiple-vertex state flip for a general graph

The bridge addition and deletion processes can be extended to a general graph, but Eqs. (S2) and (S3) have to be modified accordingly. Here we describe the extended bridge flipping processes from one configuration $\boldsymbol{c}$ to another configuration $\boldsymbol{c}'$. For simplicity we assume the input graph G to be K-regular (i.e., each vertex having K nearest neighbors). Let us denote $\theta \equiv \lceil \frac{K}{2} \rceil$. An empty vertex (say i) is regarded as a candidate start/end of a possible empty bridge if i has exactly $\theta-1$ occupied neighbors. Notice that if such a vertex i is flipped to the state $c_i = 1$ one of its empty neighbors must also be flipped. The sets of such empty terminal vertices of the initial configuration $\boldsymbol{c}$ and of the updated configuration $\boldsymbol{c}'$ are denoted as $B_{0\to1}$ and $B'_{0\to1}$, respectively. An occupied vertex j is regarded as a candidate start/end of a possible occupied bridge if (1) j has exactly θ occupied neighbors and, (2) one of these occupied neighbors (say k) has exactly θ occupied neighbors itself while all the other occupied neighbors have more than θ occupied neighbors. Notice that if j is flipped to $c_j = 1$ the occupied neighbor k must also be flipped. The sets of such occupied terminal vertices in $\boldsymbol{c}$ and $\boldsymbol{c}'$ are denoted as $B_{1\to0}$ and $B'_{1\to0}$, respectively.

To construct an empty bridge for the configuration $\boldsymbol{c}$ we proceed as follows: (1) Set index $l = 1$ and draw an empty vertex i_l from the set $B_{0\to1}$ and consider it as the start of an empty bridge. (2) Construct a set C_{i_l} for the newly added vertex i_l, which contains all the empty vertices k satisfying the following properties: (a) k is a nearest neighbor of i_l but it is not a nearest neighbor of any other existing vertices of the bridge (to avoid loop formation), (b) k has not yet been added to the bridge, and (c) k has either $\theta-1$ or $\theta-2$ occupied neighbors. If set $C_{i_l} = \emptyset$, the bridge construction is regarded as a failure and it is terminated; otherwise randomly draw an empty vertex i_{l+1} from C_{i_l} and add it to the empty chain. (3) Set $l \leftarrow l + 1$. If the last added vertex has exactly $\theta - 1$ occupied neighbors, the bridge construction is regarded as successful and it is terminated, otherwise go back to step (2) to try to further elongate the empty bridge. If this bridge construction process is successfully finished, we obtain an empty bridge $(i_1, i_2, \ldots, i_{n_b})$ involving $n_b \geq 2$ empty vertices. Because of the randomness in extending this empty bridge, we assign it a "surprising" scale as

$$W^0_{i_1,i_2,\ldots,i_{n_b}} = \prod_{l=1}^{n_b-1} |C_{i_l}| \,, \tag{S4}$$

where $|C_{i_l}|$ denotes the cardinality of vertex set C_{i_l}. Notice that the set C_{i_l} for index $l \geq 2$ is affected by the vertices $i_1, i_2, \ldots, i_{l-1}$ of the bridge.

To construct an occupied bridge for the configuration $\boldsymbol{c}$ is easier than constructing an empty bridge. Let us refer to an occupied vertex j as being critical occupied if it has exactly θ occupied

neighbors (so it has to be flipped to $c_j = 0$ if any one of its occupied neighbors is flipped). Then a candidate occupied bridge is generated in the following way: (1) Set index $l = 1$ and draw an occupied vertex i_1 from the set $B_{1\to 0}$ and consider i_1 as the start of an occupied bridge. (2) Add the only critically occupied nearest neighbor (say vertex i_2) of i_1 to the bridge and increase the index to $l = 2$. (3) If the newly added vertex i_l has only one critically occupied neighboring vertex (i.e., i_{l-1}) the candidate bridge is constructed and the process is terminated; if i_l has more than two critically occupied neighboring vertices the bridge construction is regarded as failed and it is terminated; otherwise i_i has exactly two critically occupied neighbors (one is i_{l-1}, the other one is denoted as i_{l+1}), then we add i_{l+1} to the bridge, increase index $l \leftarrow l + 1$, and repeat the last step (3) to further elongate the occupied bridge if necessary. After this bridge construction process is successfully finished, we obtain a candidate bridge $(i_1, i_2, \ldots, i_{n_b})$ involving $n_b \geq 2$ occupied vertices. To check whether this occupied chain is a valid bridge, we flip all the vertices of this chain to be empty. If every occupied nearest neighboring vertex of this chain still has θ or more occupied nearest neighbors itself after this chain has been flipped to empty, then the chain is regarded as a valid bridge and its "surprising" scale as an empty bridge is computed according to Eq. (S4), otherwise it is regarded as a failure. After this check all the vertices in the chain is flipped back to be occupied.

Given an occupation configuration $\boldsymbol{c}$, if we decide to perform a multiple-vertex flipping trial (which occurs with probability p_m), then

1. With probability $\frac{|B_{0\to 1}|}{|B_{0\to 1}|+|B_{1\to 0}|}$ it is a bridge addition trial: an empty chain $(i_1, i_2, \ldots, i_{n_b})$ of variable length $n_b \geq 2$ is generated according to the above-mentioned protocol and, if it is a valid empty bridge, the whole bridge is flipped and accepted with probability

$$A_m^{0\to 1}(\boldsymbol{c} \to \boldsymbol{c}') = \min\left(1,\ \frac{|B_{0\to 1}| + |B_{1\to 0}|}{|B'_{0\to 1}| + |B'_{1\to 0}|} W^0_{i_1,i_2,\ldots,i_{n_b}} e^{-\beta n_b}\right). \tag{S5}$$

2. With the remaining probability $\frac{|B_{1\to 0}|}{|B_{0\to 1}|+|B_{1\to 0}|}$ it is a bridge deletion trial: an occupied chain $(i_1, i_2, \ldots, i_{n_b})$ of variable length $n_b \geq 2$ is generated according to the above-mentioned protocol and, if it is a valid occupied bridge, the whole bridge is flipped and accepted with probability

$$A_m^{1\to 0}(\boldsymbol{c} \to \boldsymbol{c}') = \min\left(1,\ \frac{|B_{0\to 1}| + |B_{1\to 0}|}{|B'_{0\to 1}| + |B'_{1\to 0}|} \frac{1}{W^0_{i_1,i_2,\ldots,i_{n_b}}} e^{\beta n_b}\right). \tag{S6}$$

   Let us emphasize again that $W^0_{i_1,i_2,\ldots,i_{n_b}}$ in Eq. (S6) is the surprising scale of the resulting empty bridge $(i_1, i_2, \ldots, i_{n_b})$ *after* the flip.

D. Extending bridge-flipping into tree-flipping

The bridge-flipping process of the preceding subsection can be extended into tree-flipping process with some modifications. We define a connected subgraph of the K-regular graph as a flippable occupied tree (FOT) if the following conditions are satisfied: (1) the FOT forms a connected subgraph without any internal loops; (2) each vertex i of this FOT is occupied ($c_i = 1$) and has exactly θ occupied neighbors; (3) flipping all the vertices in this FOT will not force any other vertices in the graph to be flipped. Similarly a flippable empty tree (FET) is defined as a connected subgraph without any internal loops with the following additional properties: (1) every vertex i in this FET is empty ($c_i = 0$); (2) every leaf vertex of this FET is connected to exactly $\theta-1$ occupied external vertices (which do not belong to the FET) and one vertex in the FET; (3) every non-leaf vertex j of this FET is connected to $d_j \in \{0, 1, \ldots, \theta\}$ other vertices of the FET and exactly $\theta-d_j$ occupied external vertices.

According to the above definitions, a FOT can be flipped to be a FET without disturbing the states of all other vertices, and a FET can be flipped back to be a FOT without the need of flipping any additional empty vertices. We have implemented this tree-flipping process under the condition of detailed balance. It turns out that the resulting numerical code is much slower than that of the bridge-flipping process. When testing on the RR graph instances of degrees $K = 3, 4, 5, 6$ we found that the tree-flipping SA algorithm produces quantitatively very similar results as the bridge-flipping SA algorithm. For example, in the case of $K=5$, the dramatic energy drop occurs at $\beta_{SA} \approx 0.979$ and the final energy level is $\rho \approx 0.180$; the corresponding values for the $K=6$ case are $\beta_{SA} \approx 1.205$ and $\rho \approx 0.102$. The simulation data in Fig. 2 of the main text and Fig. S2 of the current document were obtained by the simpler bridge-flipping algorithm; while the SA results listed in Table I of the main text were obtained by the slightly better performing tree-flipping algorithm. More detailed analysis of the tree-flipping SA algorithm will be reported in a follow-up paper.

There are some non-trivial restrictions in our bridge-flipping and tree-flipping protocols which make it difficult to rigorously prove that the configuration transition matrix is ergodic for a general graph G. At the moment we are able to prove the ergodicity property only for graphs of maximum vertex degree less than 5 (see the following subsection S1 G). However, ergodicity can be guaranteed by adding some Monte Carlo transition rules or by relaxing the hard SDA constraints into soft energy penalty terms. The next two subsections describe such alternative SA protocols. As expected, the simulation results obtained by these new SA algorithms are similar to our bridge-flipping and

tree-flipping SA algorithms, see subsection S1 G.

E. Additional multiple-vertex flipping rules

Besides the bridge-flipping and tree-flipping rules, we consider two additional multiple-vertex flipping rules, one of them is referred to as cascade-flipping and the other as creation-flipping. The purposes of these two processes is to guarantee the ergodicity of the SA dynamics and validate the robustness of the SA simulation results. These are not employed in our default SA simulations due to their heavy computational cost.

The cascade-flipping rule goes as follows. First an occupied vertex j which is connected to at least one critically occupied vertex (say k), is chosen uniformly at random from the set of all such occupied vertices. The state of the chosen vertex j is then flipped and clamped to the value $c_j = 0$. This forced flip destabilizes critically occupied neighboring vertices (such as k) collapsing to the zero state. These induced flips may in turn destabilize more occupied vertices. After this cascading process finally stops, there are two possibilities: either all the initially occupied vertices in the SDA configuration become empty (zero-state), or there are still some occupied vertices in the perturbed configuration (see subsection S1 G for additional discussions). If the former case (all-zero) occurs, the cascading process is rejected and the initial SDA configuration is kept, while if the second case occurs, the cascading process is accepted and the final configuration becomes the new SDA graph configuration. It is easy to see that this cascade-flip process may extensively decrease the energy of SDA configurations.

The creation-flipping process goesin the opposite direction to the cascade-flipping process and aims at increasing the number of occupied vertices. First an empty vertex j which is surrounded by less than $\frac{d_j}{2}$ occupied vertices is selected uniformly at random from the set of all such zero-state vertices. Then this vertex j is flipped and clamped to the value $c_j = 1$. To satisfy the SDA condition some of the empty neighbors of j are then randomly chosen and flipped to an occupied state ($c = 1$), until the SDA constraint of j is satisfied. Each newly flipped vertex is then examined (in a random order) in the same manner and the induced $0 \to 1$ flipping process is continued if necessary to satisfy the SDA rule for the newly occupied vertices. After this process stops, a new SDA configuration with an increased number of occupied vertices is constructed. Denote by Δn the total number of newly occupied vertices. We accept this new configuration as the updated configuration of the system with probability $e^{-\beta \Delta n}$ and reject it with probability $1 - e^{-\beta \Delta n}$. Notice that this creation-flip process might cause an extensive increase in the energy

of the SDA configuration, especially when the value of β is small.

The cascade-flipping process deletes a connected subgraph of occupied vertices from the current SDA configuration, while the creation-flip process adds a connected subgraph of occupied vertices to it. With these two additional state transition rules, the Monte Carlo dynamics is guaranteed to be ergodic in the whole SDA configuration space.

In each elementary SA updating process, the probability of carrying out a cascade-flipping action is set to be p_{cas}, and that of a creation-flipping action is set to be p_{add}. We did not enforce detailed balance between the cascade-flip and creation-flip processes due to the high computational cost needed to determine precisely the values of acceptance ratios. This might not be critical, since the condition of detailed balance is not absolutely necessary for obtaining low-energy configurations. Here we simply set $p_{cas} = p_{add}$ in our simulations. The corresponding bridge-flipping (or tree-flipping) probability is set to $p_m = \frac{1}{2} - p_{cas} - p_{add}$, while the single-vertex flipping probability is still $p_s = \frac{1}{2}$. In the default case of $p_{cas} = p_{add} = 0$, we have $p_s = p_m = \frac{1}{2}$.

F. SA with energy penalty: Relaxation of hard constraints on SDA vertices

The above SA protocols are conducted with the Hamiltonian $E(\boldsymbol{c}) = \sum_i \delta^1_{c_i}$ subject to the following hard constraints on every vertex in the SDA, i.e.,

$$\sum_{j\in\partial i} c_j \geq \frac{d_i}{2}\,, \qquad \forall i \text{ with } c_i = 1\,. \tag{S7}$$

In this case, all configurations visited by the SA algorithm with single-vertex state flip (i.e. the algorithm described in Sec. S1 A) are connected by paths of valid SDA configurations in the state space. It may happen that some SDA configurations cannot be visited by the SA dynamics even after a long time, if they are enclosed by invalid SDA configurations in the state space. This implies that the single-vertex state flip algorithm may be *non-ergodic* and incapable of visiting all valid configurations. In order to show that the failure of SA to obtain ground state solutions, to be discussed in the next subsection, is not due to the non-ergodicity of the algorithm, we replace the hard constraints in Eq. (S7) by *soft constraints* through the modified (relaxed) Hamiltonian:

$$E_r(\boldsymbol{c}) = \sum_i \delta^1_{c_i} + \alpha \sum_i \delta^1_{c_i} \tilde{\Theta}\Big(\frac{d_i}{2} - \sum_{j\in\partial i} c_j\Big)\,, \tag{S8}$$

where the step function $\tilde{\Theta}(x)$ is defined to be $\tilde{\Theta}(x) = 1$ if $x > 0$ and $\tilde{\Theta}(x) = 0$ if $x \leq 0$. When $\alpha \to \infty$, the system reduces to the original system with hard constraints. On the other hand, as α decreases, the system gradually explores also invalid SDA configurations. As a result, the SA

algorithm which minimizes $E_r(\boldsymbol{c})$ with a finite α does not necessarily result in a valid SDA configuration, but the single-vertex flipping process becomes ergodic since the hard constraints Eq. (S7) are relaxed and the system can visit all the 2^N possible configurations. We thus perform SA with $E_r(\boldsymbol{c})$ and a finite α value, and then reduce the resulting, potentially invalid, SDA configurations to valid ones by repeatedly re-labeling vertices with $c_i = 1$ that do not satisfy Eq. (S7) to state $c_i = 0$. In many cases, this reduction procedure leads to the removal of all vertices with $c_i = 1$, resulting in an all-zero state with no SDA. The results obtained by this algorithm are discussed in the next subsection and are compared to the results obtained for the single-vertex and multiple-vertex state flip SA algorithms.

G. Discussions on the performance of SA

The default SA dynamical results (with $p_s = p_m = \frac{1}{2}$) obtained for random K-regular graphs are shown in Fig. 2 and Fig. S2. When each vertex has only $K = 3$ (Fig. 2a) or $K = 4$ (Fig. S2a) nearest neighbors, the SA trajectory can successfully reach a minimum alliance solution, after experiencing an abrupt drop in energy density ρ, at a certain critical value of inverse temperature β predicted by the cavity theory (marked by the vertical dashed line of Fig. 2a and Fig. S2a). The simulated annealing behaviors observed on the 3- and 4-RR graphs indeed fully agree with the theoretical prediction. This algorithmic success can be well explained.

Given an occupation configuration $\boldsymbol{c}$ we refer to a vertex i as being critical if this vertex is occupied ($c_i = 1$) and it has exactly $\theta = \lceil \frac{K}{2} \rceil$ occupied nearest neighbors. A critical vertex will collapse to the empty state if any one of its occupied nearest neighbors if flipped to be empty. Since $\theta = 2$ in the cases of 3- and 4-RR graphs, a critical vertex i has at most two critical nearest neighbors and so its flipping will immediately affect at most two other occupied vertices. If vertex j is such a critical nearest neighbor of i, it will have at most one other critical nearest neighbor besides i, so the induced flipping of j will immediately affect at most one additional occupied vertex, and the same applies for the critical neighbor of j and so on. By this analysis we see the critically occupied vertices of $\boldsymbol{c}$ form some simple paths (without self-loops) which do not share any vertex. The occupied bridges sampled by the SA algorithms are just some of these critical paths. If such an occupied chain is flipped as a whole, a new occupation configuration $\boldsymbol{c}'$ of lower energy will be obtained. On the other hand, suppose there is an empty vertex j which has only a single occupied nearest neighbor and we flip j to be occupied (i.e., from $c_j = 0$ to $c_j = 1$). Then we only need to flip one of its empty nearest neighbors (say k) to make j satisfy the constraint of

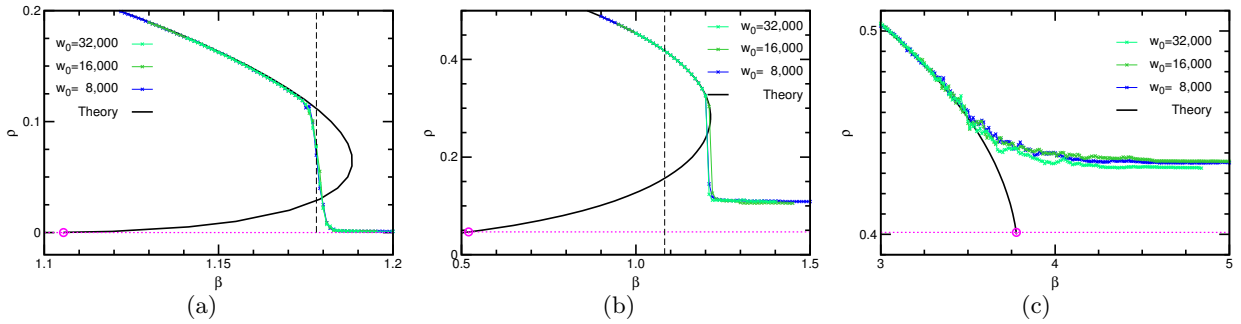

Figure S2: The same as Fig. 2 of the main text. Simulated annealing results on a single RR graph of size $N = 10^4$ and degrees $K = 4$ (a), $K = 6$ (b), and $K = 25$ (c) are compared with theoretical predictions. Evolution trajectories obtained at three different waiting times w_0 are shown. The inverse temperature is denoted by β while ρ is the relative size of alliances. In each panel the bold solid line represents the theoretical curve of ρ versus β, and the circle and dotted horizontal line mark the predicted ground-state energy density. An equilibrium discontinuous phase transition is predicted to occur for the RR ensembles of $K \leq 22$. The phase transition point, obtained from the corresponding free energy values, is marked by the dotted vertical line in (a) and (b).

being in the alliance. If vertex k again only has one occupied nearest neighbor (which is j), then we only need to flip one of the empty nearest neighbors to stabilize k, and the same applies for the neighbors of k and so on. After this chain extension process stops, a new occupation configuration $\boldsymbol{c}'$ of increased energy is reached.

By repeatedly applying the above-mentioned chain flipping and single-vertex flipping processes, any occupation configuration of a 3- or 4-RR graph can be reached from any another occupation configuration, meaning that the algorithm can reach all configurations of the system and it is an ergodic algorithm. To guarantee detailed balance property of the SA dynamics, we have further restricted the flipped chain to be a bridge (there should be no internal loop among the vertices of this chain, and flipping of this chain should not cause any of the connected occupied vertices to be unstable) but these restrictions do not affect the ergodic property of the SA dynamics. In a random graph the typical length of a shortest-distance path between two vertices grows logarithmically with the graph size N. We therefore expect the energy gap of flipping an empty bridge to be at most of order $\log(n_b)$, with n_b being the bridge length. In our simulations n_b exceeded 20 only very rarely. We have formulated a percolation theory (to be described in a following paper) to compute the mean value of n_b; this theory predicts that, for 3- and 4-RR graphs, n_b is only of $O(1)$ even for an infinite graph ($N \to \infty$). The energy barrier of bridge flipping can therefore be easily overcome. This property together with the ergodicity property of SA for the 3- and 4-RR graphs explain why

the SA evolution trajectories in Fig. 2a and Fig. S2a abruptly drop at the theoretical predicted phase transition point to visit a ground state.

Results for RR graphs of degrees $K = 5$ and $K = 6$, shown in Fig. 2b and Fig. S2b, exhibit an abrupt drop of energy density ρ during the SA evolution process; this does not occur at the predicted equilibrium phase transition point (the vertical dashed line of Fig. 2b and Fig. S2b), but close to the predicted entropy inflection point. After this much delayed drop in energy the SA evolution trajectory still fails to reach the energy level of ground states but is trapped at a much higher energy level. It seems that the energy barriers are high in these graph instances and the SA evolution dynamics with only single-vertex and bridge (or tree) flips is unable to overcome these barriers, leading to effective ergodicity-breaking in the SA process.

To see why ergodicity in the configuration space of the K-RR graph ($K \geq 5$) might be severely broken at low energy levels, let us investigate the consequence of flipping an occupied vertex i (from $c_i = 1$ to $c_i = 0$). If an occupied nearest neighboring vertex j of i is critical (that is, having exactly θ occupied nearest neighbors), j will no longer be marginally stable and it will collapse to the empty state ($c_j = 0$). Since $\theta \geq 3$ vertex j may itself be connected to more than one critically occupied vertex besides j, and its collapse may then induce the collapse of two or more (up to $\theta - 1$) critically occupied nearest neighbors, and so on. When this avalanche process finally stops and we count the remaining occupied vertices, with high probability the whole alliance solution has collapsed! This single-vertex flipping may therefore induce a complete collapsing behavior as demonstrated in Fig. S3b on a 5-RR graph instance, and it is prohibited because the all-empty configuration does not correspond to a valid alliance solution. This global collapsing behavior is dramatically different from the situation observed on a 3-RR graph (Fig. S3a), for which the avalanche size is always finite (< 50) at any value of β.

For the 5–RR graph, as long as the inverse temperature β exceeds 0.8, we observed that a finite fraction of the occupied vertices in *every* visited equilibrium configurations are completely blocked (flipping any one of these occupied vertices will cause the collapse of the whole alliance solution). We have developed a percolation theory to quantitatively understand this strong blocking phenomenon (to be reported in the follow-up paper). The equilibrium dynamics of the system is therefore severely restricted. For such a blocked vertex (say i) to be flippable, the system has to rearrange itself (through many local single-vertex or multiple-vertex flips) into a suitable configuration in which i is no longer blocked; but with the relaxation of vertex i some other vertices will be blocked and the evolution trajectory will still be strongly restricted. In other words, there is a high degree of dynamical heterogeneity among the vertices: some of the vertices can be

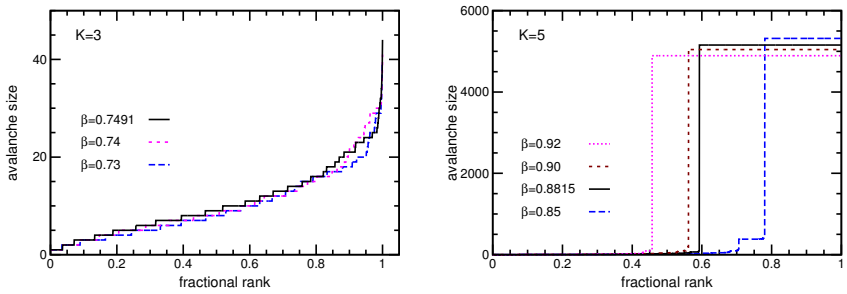

Figure S3: The size of avalanches induced by flipping a single occupied vertex i on an alliance configuration $\boldsymbol{c}$. The size a_i of this avalanche is defined as the total number of flipped vertices (including i). The n occupied vertices in $\boldsymbol{c}$ are ranked with index $r = 1, 2, \ldots, n$ according to the avalanching effect and the relative rank is simply r/n. The results of avalanche size for (a) a 3-RR graph instance of size $N = 10^4$, at three different values of β (the predicted phase transition point is $\beta_c = 0.7491$), with the alliance size n being $n = 2129$ ($\beta = 0.73$), $n = 1930$ ($\beta = 0.74$) and $n = 2017$ ($\beta = 0.7491$); and (b) a 5-RR graph of size $N = 10^4$, at four different β values ($\beta_c = 0.8815$), with alliance size being $n = 5318$ ($\beta = 0.85$), $n = 5156$ ($\beta = 0.8815$), $n = 5043$ ($\beta = 0.90$) and $n = 4894$ ($\beta = 0.92$). The big jumps in (b) correspond to all the vertices in the graph being in the empty state.

easily flipped while the others are completely blocked, and every vertex changes between these two coarse-grained states over time. The entropic barrier associated with an extensive number of blocked vertices may make it impossible for the SA evolution process to realize the huge energy drop at the predicted discontinuous phase transition point β_c. Instead the SA dynamics enters into the "super-cooled" non-equilibrium region (see Fig. 2b and Fig. S2b) as β exceeds β_c.

The simulation results of Fig. S2 on a RR graph of degree $K = 25$ demonstrate a smooth decrease of energy density ρ with inverse temperature β, in agreement with the theoretical prediction of the absence of a discontinuous phase transition in RR graph ensembles of degree $K \geq 23$. However, at $\beta \approx 3.5$ the SA evolution trajectories start to deviate from the theoretical $\rho(\beta)$ curve, possibly due to the waiting times w_0 used in the SA dynamics becoming shorter than the characteristic system relaxation time. It may also be possible that the low-energy configurations (with $\rho < 0.45$) of this 25-RR graph instance are in the spin glass phase. This possibility deserves to be thoroughly explored in future investigations.

We validated that adding more sophisticated multiple-vertex flipping (cascade-flipping and creation-flipping) rules does not qualitatively improve the performance of the SA algorithm. For example, as shown in Fig. S4a, when cascade-flipping is introduced to the SA algorithm alongside single-vertex flipping and tree-flipping, the SA dynamics still fails to reach the ground-state energy

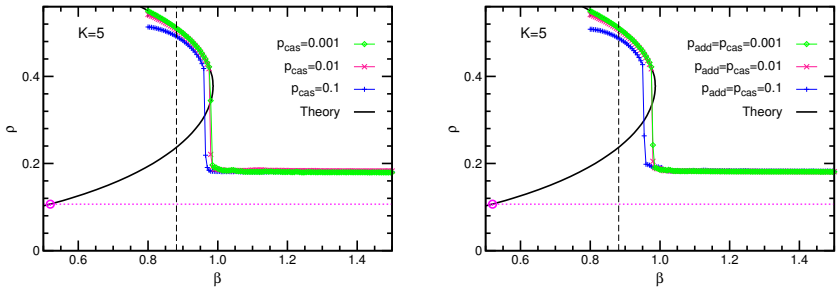

Figure S4: Representative simulation results obtained by the SA algorithm with multiple-vertex flipping protocols. The RR graph has $N = 10^4$ vertices of degree $K = 5$; ρ is the fraction of occupied vertices during the evolution process, and β the inverse temperature. The SA dynamics waits $w_0 = 10^4$ time steps (i.e., performing $10^4 N$ updating trials) at each β value. (a) Cascade-flipping (probability $p_{cas} \in \{0.001, 0.01, 0.1\}$) is combined with single-vertex flipping (probability $p_s = 1/2$) and tree-flipping (probability $p_m = 1/2 - p_{cas}$) in the SA algorithm. (b) Cascade-flipping (probability p_{cas}) and creation-flipping (probability $p_{add} = p_{cas}$) are employed together with single-vertex (probability $p_s = 1/2$) and tree-flipping (probability $p_m = 1/2 - p_{cas} - p_{add}$) processes. In each panel the bold solid line represents the theoretical curve of ρ versus β, the circle and dotted horizontal line mark the predicted ground-state energy density, and the dashed vertical line marks the predicted equilibrium discontinuous phase transition point.

level. Adding both creation-flipping and cascade-flipping to the SA algorithm does not help either (Fig. S4b).

Finally, we report the results of the SA algorithm with relaxed Hamiltonian $E_r(\boldsymbol{c})$ of Eq. (S8), i.e. when an energy penalty is used instead of a hard constraint for vertices violating the SDA condition Eq. (S7). In Fig. S5a, we show the fraction of occupied vertices, i.e. $\sum_i \delta^1_{c_i}/N$, as a function of β for a large RR graph with $K = 5$. We remark that the identified configurations are not necessarily valid SDAs, as some vertices may violate the hard constraints of Eq. (S7). As we can see, although the configurations are not necessarily SDA, the number of occupied vertices roughly follow the theoretical prediction of the SDA size and shows an abrupt drop when β is close to the entropy inflection point, similar to the results obtained by multiple-vertex flipping algorithm and shown in Fig. 2b of the main text, which are also for $K = 5$. Beyond the entropy inflection point, the total number of occupied vertices becomes zero with $\alpha = 5$ in the relaxed Hamiltonian $E_r(\boldsymbol{c})$ of Eq. (S8), implying that the SA dynamics gives a solution with no SDA (i.e. $\rho = 0$) after enforcing the hard constraints Eq. (S7). With larger values of α and hence a stronger enforcement of the hard constraints, the SA dynamics recovers a non-zero number of occupied vertices beyond the entropy inflection point, but the relative sizes of obtained configurations are much higher than

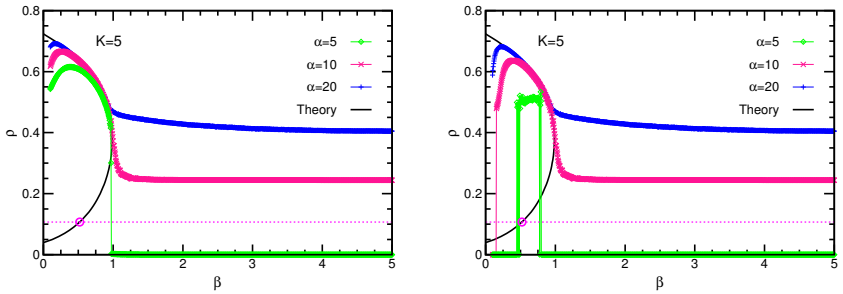

Figure S5: Representative simulation results obtained on the modified model Eq. (S8) by the single-vertex flipping SA algorithm. (a) The fraction ρ of occupied vertices in potentially invalid SDA configurations, and (b) the relative size ρ of SDA after a reduction procedure is performed to obtain valid SDA configurations, as a function of inverse-temperature β. Results were obtained on a single RR graph of size $N = 10^4$ and degree $K = 5$. The evolution trajectories were obtained by using a waiting time $w_0 = 10^5$, i.e. with $10^5 N$ flip trials at each value of β. The results for three different values of $\alpha = 5, 10$ and 20 in the relaxed Hamiltonian $E_r(\boldsymbol{c})$ of Eq. (S8) are shown. In each panel the bold solid line represents the theoretical curve of ρ versus β, and the circle and dotted horizontal line mark the predicted ground-state energy density.

the predicted ground state energy density and are similar to the results shown in Fig. 2b of the main text.

Since the configurations identified by the algorithm are not necessarily SDAs, we prune vertices of the invalid SDA configurations which violate the SDA constraints to create valid ones. This is done by repeatedly re-labeling vertices with $c_i = 1$ that do not satisfy Eq. (S7) as $c_i = 0$. If a valid SDA configuration is identified after the pruning procedure, we show the resulting value of SDA relative size ρ in Fig. S5b; otherwise, if no valid SDA configuration can be found, we show $\rho = 0$. In this case, the value of ρ shown in Fig. S5b should be either equal to or smaller than the number of occupied vertices shown in Fig. S5a. As we can see, using the pruning procedure before the entropy inflection point, for $\alpha = 5$, a lower SDA relative size is obtained compared to the equilibrium theoretical value (but is much higher than the ground-state value); however, the SA algorithm fails again to identify the ground-state SDA beyond the inflection point. For $\alpha = 10$ and $\alpha = 20$, the SDA relative sizes behave similarly, as a function of β, to the multiple-vertex flipping SA algorithm, as shown in Fig. 2b of the main text. Qualitatively similar results shown in Fig. S5 are obtained for other values of the parameter α (it turns out that the optimal value is $\alpha \approx 8$, with achieved minimum relative SDA size $\rho \approx 0.195$). We therefore conclude that although the SA algorithm with a relaxed Hamiltonian is ergodic, it cannot identify the ground-state SDA configurations.

S2. THEORETICAL EXPRESSIONS FOR A REGULAR-RANDOM (RR) GRAPH

The BP equations (3) of the main text can be solved iteratively (see the following section). For a RR graph of degree K, due to the uniformity of vertex properties; it turns out that the fixed-point cavity probability distributions on all edges are identical. Therefore the BP equations (3) for the RR graph ensemble can be simplified to

$$q^{(0,0)} = q^{(0,1)} = \frac{1}{z}(q^{(0,0)} + q^{(1,0)})^{K-1} , \tag{S9a}$$

$$q^{(1,0)} = \frac{e^{-\beta}}{z} \sum_{d \geq \frac{K}{2}}^{K-1} C_{K-1}^{d} (q^{(1,1)})^{d} (q^{(0,1)})^{K-1-d} , \tag{S9b}$$

$$q^{(1,1)} = \frac{e^{-\beta}}{z} \sum_{d \geq \frac{K}{2}-1}^{K-1} C_{K-1}^{d} (q^{(1,1)})^{d} (q^{(0,1)})^{K-1-d} , \tag{S9c}$$

where $C_n^m \equiv \frac{n!}{m!(n-m)!}$, and z is the normalization constant. The corresponding marginal occupation probability (simply ρ) for a vertex is

$$\rho = \frac{e^{-\beta} \sum\limits_{d \geq \frac{K}{2}}^{K} C_{K}^{d} (q^{(1,1)})^{d} (q^{(0,1)})^{K-d}}{(q^{(0,0)} + q^{(1,0)})^{K} + e^{-\beta} \sum\limits_{d \geq \frac{K}{2}}^{K} C_{K}^{d} (q^{(1,1)})^{d} (q^{(0,1)})^{K-d}} . \tag{S10}$$

Equations (S9a)-(S9c) can be analytically solved for the simplest non-trivial case of degree $K = 3$, and the solution demonstrates the existence of an inflection point in the entropy–energy profile. Let us first simplify the notation by introducing

$$a = q^{1,1} , \quad b = q^{0,1} , \quad c = q^{1,0} , \quad d = q^{0,0} . \tag{S11}$$

For the case of $K = 3$ the BP equation (S9) can be written as

$$b = d = \frac{1}{z}(c + d)^2 , \quad a = \frac{e^{-\beta}}{z}(a^2 + 2ab) , \quad c = \frac{e^{-\beta}}{z} a^2 . \tag{S12}$$

One can re-arrange Eqs. (S9a)-(S9c) to obtain the exact solution of cavity probabilities, and subsequently the free energy and the entropy. In this case, by using Eq. (S12), we obtain

$$\frac{a}{c} = 1 + 2\frac{b}{a} , \tag{S13}$$

$$\frac{b}{a} = \frac{\left(\frac{b}{a} + \frac{c}{a}\right)^2}{e^{-\beta}\left(1 + 2\frac{b}{a}\right)} . \tag{S14}$$

Let us denote $x = a/b$. From the above equations we obtain the following equation for x

$$(x^2 + x + 2)^2 - e^{-\beta}(x + 2)^3 = 0 . \tag{S15}$$

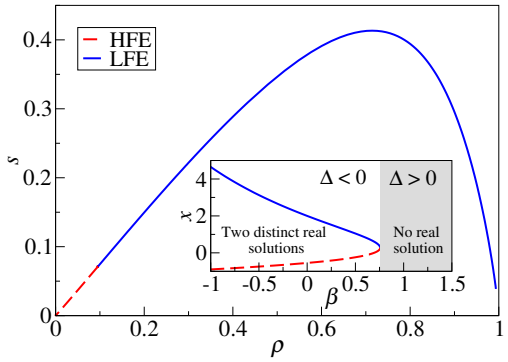

Figure S6: The non-concave entropy density function $s(\rho)$ for the RR graphs of degree $K = 3$, obtained from Eqs. (S16a) and (S16c), with the solution of x from Eq. (S15). Inset: the solution of x given by Eq. (S15), which shows that there is a range of β values with no real solution for x. Similar to Fig. 3 of the main text, the corresponding BP fixed-point solutions form higher (HFE) and lower-free-energy (LFE) branches.

The energy density ρ, the free energy density f, and the entropy density s can also be expressed in terms of x as

$$\rho = \frac{e^{-\beta}(x^3+3x^2)}{\left(\frac{x^2}{x+2}+1\right)^3 + e^{-\beta}(x^3+3x^2)} , \tag{S16a}$$

$$f = -\frac{1}{\beta}\ln\Big[\Big(\frac{x^2}{x+2}+1\Big)^3 + e^{-\beta}(x^3+3x^2)\Big] + \frac{3}{2\beta}\ln\Big[1+x^2+\frac{2x^2}{x+2}\Big] , \tag{S16b}$$

$$s = \beta(\rho - f) . \tag{S16c}$$

By solving the quartic equation in (S15) at a given value of β, one can obtain both lower and higher free-energy solutions, real and complex. Since only the real solutions are relevant in the present case, we first write the determinant Δ of Eq. (S15) as $\Delta = \Delta_1^2 - 4\Delta_0^3$, where $\Delta_0 = -72e^{-\beta} + 49$ and $\Delta_1 = 432e^{-2\beta} + 1512e^{-\beta} - 686$. One can then solve Eq. (S15) explicitly for β when $\Delta = 0$, which gives

$$\beta = -\ln\Big(\frac{19\sqrt{57}-135}{18}\Big) \approx 0.757 . \tag{S17}$$

When the determinant of the quartic equation $\Delta > 0$, i.e. $\beta > 0.757$, there is no real solution for x in Eq. (S15) and consequently for the cavity probabilities. On the the other hand, there are two distinct solutions when $\Delta < 0$, i.e. $\beta < 0.757$ (see Fig. S6). By using Eqs. (S16a)–(S16c), we can plot the entropy–energy profile $s(\rho)$ with the two solutions of x sharing the same temperature range $\beta < 0.757$. The concave branch of $s(\rho)$ is obtained from one of the solutions, while the

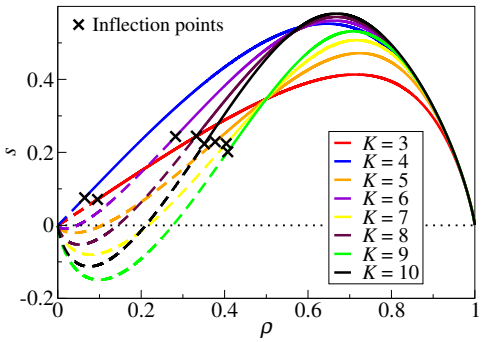

Figure S7: The analytical results of the entropy–energy profile $s(\rho)$ for RR graphs with $K = 3$ to $K = 10$, obtained by the cavity theory in Eq. (2)-(6) of the main text. The inflection points are indicated by the cross symbols $\times$, and the dashed lines correspond to the convex regime of $s(\rho)$.

other leads to the convex branch. The inflection point of $s(\rho)$ locates at the value of ρ for which $\beta = 0.757$.

As for related work, we notice that Ref. [1] discussed the inflection point of the inverse temperature, but not that of the entropy, and specifically conclude that the entropy function will be concave in the thermodynamic limit. For the SDA system studied here, the non-concavity of the entropy function persist in the thermodynamic limit.

In addition to the emergence of an inflection point ($\rho = \rho_x$), the entropy density at low ρ values ($\rho < \rho_o$) becomes negative and unphysical for RR graphs with $K \geq 5$, as shown in Fig. S7. Since the number of configurations at a given energy density ρ is of order $e^{Ns(\rho)}$, a negative value of entropy density indicates that low-energy configurations of $\rho < \rho_o$ are non-existent in a typical RR graph instance. Therefore, we define the SDA ground states to be the states of minimal SDA with non-negative entropy. According to this definition, since the entropy for the cases of $K = 3, 4$ is always positive (see Fig. S7), the SDA ground states are characterized by $\rho \gtrsim 0$. As discussed in the main text, the ground states for $K = 3, 4$ are states with occupied triangular loops; if we denote n to be the number of alliance nodes, the ground states are characterized by $n = 3$, such that $\rho_o = n/N \gtrsim 0$ in a system with large N. In this case, $s(\rho_o)$ is infinitesimally positive, implying that there may be more than one ground state, i.e. more than one state with a different occupied triangle loops, which is consistent with the results of the statistics of loops in RR graphs obtained in [2].

Coming back to the cases of negative entropy, we note that for cases of $K \geq 5$, there is a negative-entropy regime just before $\rho = 0$, implying that states with $\rho \gtrsim 0$ have negative entropy

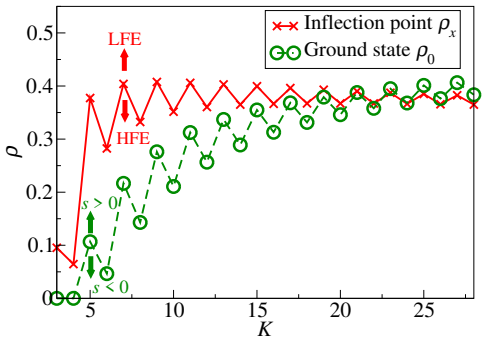

Figure S8: The energy density ρ_x of the inflection point (crosses) and the minimum energy density ρ_o (circles), for the RR graph ensemble of degree $K \in \{3, 4, \ldots, 28\}$. ρ_x separates the lower-free-energy (LFE) branch from the higher-free-energy (HFE) branch; ρ_o is determined by the condition of zero entropy density.

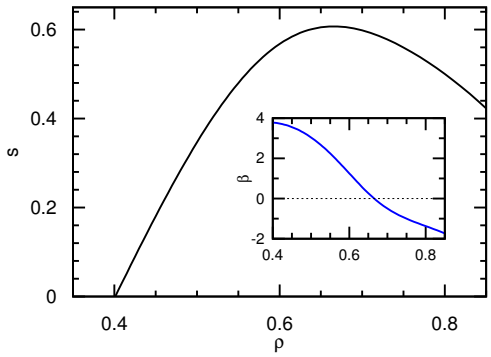

Figure S9: The concave entropy density $s(\rho)$ for the RR graph ensemble of degree $K = 25$. The inset shows the slope $\mathrm{d}s(\rho)/\mathrm{d}\rho$ of the entropy density.

and unphysical and thus are not the ground states of the system. This interpretation of the negative-entropy states with $\rho \gtrsim 0$ is consistent with our analysis of the unlikely presence of clique of size $n = 4$ in RR graphs with $K = 5$, shown in Sec. S4. This further implies that for cases of $K \geq 5$, the SDA ground states are those states with the minimal values of ρ just beyond the negative entropy regime. By allowing the possibility of replica-symmetry-breaking at the vicinity of ρ_o, the precise values of the minimum energy density ρ_o may be further improved (see, e.g., [3, 4]). We leave this RSB exploration for future studies.

We have determined the values of ρ_x and ρ_o for the RR graph ensembles with K ranging from $K = 3$ to $K = 28$, see Fig. S8. Both ρ_x and ρ_o depend on the even-odd parity of K and show oscillating behavior. We find that $\rho_x > \rho_o$ only for $K \leq 22$. When $K \geq 23$, we have $\rho_x < \rho_o$, so the entropy density is concave in the whole physically relevant range of $\rho \geq \rho_o$ (see Fig. S9 for the example of $K = 25$).

S3. SOLVING THE BELIEF-PROPAGATION EQUATION

In addition to the method used in the preceding section, we also employ conventional methods [4] for solving the BP equation [Eq. (3) of the main text].

A. With fixed inverse temperature β

At a given fixed value of β, we iterate the BP equation on a single graph G to obtain a fixed-point solution. At each elemental iteration process a vertex j is randomly chosen from all N vertices of the graph, and the cavity probability distributions $q_{j\to i}^{c_j,c_i}$ on the edges between j and all its nearest neighbors i are updated according to Eq. (3). When G is a RR graph we experience that this BP evolution converges to a fixed point within about $100N$ elemental updates, and this fixed point is uniform in that the cavity probability distributions are identical for all the graph edges.

To get ensemble-averaged results for random graphs characterized by certain vertex degree profile, we also perform population dynamics simulations based on Eq. (3). In the case of the RR graph ensemble, we first construct a long array of cavity probability distributions $q_{j\to i}^{c_j,c_i}$; then we repeatedly update it by (1) drawing $K-1$ cavity distributions uniformly at random from this array as inputs to Eq. (3) to generate a new cavity distribution, and (2) replace an old cavity distribution in the array (chosen uniformly at random) by this new cavity distribution. This population dynamics also drives the population of cavity probability distributions to the uniform population (all the elements being identical) for the RR graph ensemble. The ensemble-averaged and single-graph BP results therefore are in complete agreement.

B. With fixed energy density ρ

To perform BP iteration at fixed energy density ρ, we need to slightly modify Eq. (3) as follows

$$w_{j\to i}^{0,0} \equiv w_{j\to i}^{0,1} = \prod_{k\in\partial j\backslash i} (q_{k\to j}^{0,0} + q_{k\to j}^{1,0}) \,, \tag{S18a}$$

$$w_{j\to i}^{1,0} = \sum_{\boldsymbol{c}_{\partial j\backslash i}} \Theta\Big(\sum_{k\in\partial j\backslash i} c_k - \frac{d_j}{2} \Big) \prod_{k\in\partial j\backslash i} q_{k\to j}^{c_k,1} \,, \tag{S18b}$$

$$w_{j\to i}^{1,1} = \sum_{\boldsymbol{c}_{\partial j\backslash i}} \Theta\Big(\sum_{k\in\partial j\backslash i} c_k + 1 - \frac{d_j}{2} \Big) \prod_{k\in\partial j\backslash i} q_{k\to j}^{c_k,1} \,, \tag{S18c}$$

where $w^{0,0}_{j\to i}$, $w^{0,1}_{j\to i}$, $w^{1,0}_{j\to i}$, and $w^{1,1}_{j\to i}$ are four auxiliary weight messages from vertex j to its nearest neighbor i. We denote these four real quantities collectively as $\boldsymbol{w}_{j\to i}$. Similarly, we define the marginal weights $\boldsymbol{w}_j \equiv (w^0_j, w^1_j)$ of vertex j as

$$w^0_j \equiv \prod_{k\in\partial j} (q^{0,0}_{k\to j} + q^{1,0}_{k\to j}) \ , \tag{S19a}$$

$$w^1_j \equiv \sum_{\boldsymbol{c}_{\partial j}} \Theta\big(\sum_{k\in\partial j} c_k - \frac{d_j}{2}\big) \prod_{k\in\partial j} q^{c_k,1}_{k\to j} \ , \tag{S19b}$$

In each BP iteration the following actions are taken: (1) we update the output messages $\boldsymbol{w}_{j\to i}$ and $\boldsymbol{w}_{i\to j}$ for each pair of edges (i,j) of the graph according to Eq. (S18), and the marginal weights $\boldsymbol{w}_j$ for all the vertices j according to Eq. (S19); (2) and determine the value of the inverse temperature β as the root of the following equation

$$\rho = \sum_{j=1}^{N} \frac{e^{-\beta} w^1_j}{e^{-\beta} w^1_j + w^0_j} \ ; \tag{S20}$$

and (3) we re-calculate the cavity probability distributions $q_{j\to i}$ between all the nearest-neighboring vertices using the new β:

$$q^{0,0}_{j\to i} \equiv q^{0,1}_{j\to i} = \frac{1}{z_{j\to i}} w^{0,0}_{j\to i} \ , \tag{S21a}$$

$$q^{1,0}_{j\to i} = \frac{e^{-\beta}}{z_{j\to i}} w^{1,0}_{j\to i} \ , \tag{S21b}$$

$$q^{1,1}_{j\to i} = \frac{e^{-\beta}}{z_{j\to i}} w^{1,1}_{j\to i} \ , \tag{S21c}$$

where $z_{j\to i}$ is the normalization constant.

Similar to the discussions in the preceding subsection, we also iterate the modified BP equations (S18)–(S21) by population dynamics to get ensemble-averaged results for the random SDA problem. For the RR graph ensembles the population dynamics results are in full agreement with BP results on single graph instances.

S4. SOME SIMPLE PROBABILISTIC ARGUMENTS CONCERNING ENTROPY AND ENERGY

The entropy density of the SDA problem is revealed by the cavity theory to be non-concave. Here we present a simple probabilistic theory to further confirm this non-concavity.

Consider a random regular graph of degree K. The total number of occupation configurations $\boldsymbol{c}$ with $N\rho$ occupied vertices and $(1-\rho)N$ empty vertices is simply $C_N^{N\rho}$. The probability that a

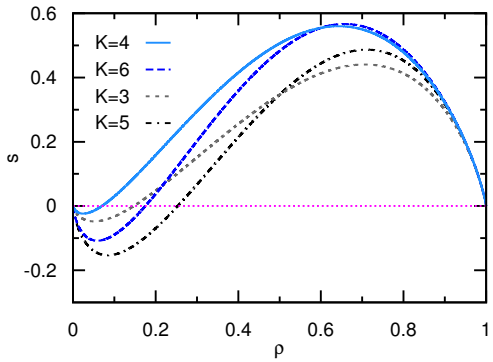

Figure S10: The non-concave entropy density function $s(\rho)$ as predicted by the simple probabilistic theory [Eq. (S24)] for the RR graph ensemble of degree $K \in \{3, 4, 5, 6\}$.

randomly chosen configuration from this subset being an alliance is

$$\left[\sum_{d\geq\frac{K}{2}}^{K} \frac{K!}{d!(K-d)!}\rho^d(1-\rho)^{K-d}\right]^{N\rho}. \tag{S22}$$

Therefore the mean number of alliances with a given relative size ρ is estimated to be

$$\Omega(\rho) = C_N^{N\rho}\left[\sum_{d\geq K/2}^{K} \frac{K!}{d!(K-d)!}\rho^d(1-\rho)^{K-d}\right]^{N\rho}. \tag{S23}$$

At the thermodynamic limit $N \to \infty$, the entropy density $s(\rho) \equiv \frac{1}{N}\ln\Omega(\rho)$ is then estimated to be

$$s(\rho) = -\rho\ln\rho - (1-\rho)\ln(1-\rho) + \rho\ln\left[\sum_{d\geq\frac{K}{2}}^{K} \frac{K!}{d!(K-d)!}\rho^d(1-\rho)^{K-d}\right]. \tag{S24}$$

This simple probabilistic theory predicts that the entropy density function $s(\rho)$ is convex when ρ is small, see Fig. S10. Furthermore it predicts $s(\rho)$ to be negative for $0 < \rho < \rho_o$ with ρ_o being some K-dependent threshold value, which means that there should not be any defensive alliance with relative size $\rho < \rho_o$. These predictions are in qualitative agreement with the results of the RS cavity theory.

The size n of a minimum alliance for a 3- or 4-RR graph is found by the SA algorithm to be $n = 3$, namely, the minimum alliance is a triangle. On the other hand, both theory and SA simulations suggest that the minimum alliance size of a 5-RR graph is extensive. One would wonder why a small change in the value of K from 4 to 5 results in an extensive gap in the size of alliance size n. Given a 5-RR graph of large size N, why should we not expect to find a clique of size $n = 4$ (with each vertex connecting to all the three other vertices of this clique) to serve as a minimum alliance? Here we offer an intuitive explanation. The expected number of a clique of size $n = 4$ in

a 5-RR graph is

$$\binom{N}{4} \frac{\binom{N-4}{2}}{\binom{N-1}{5}} \frac{\binom{N-4}{2}}{\binom{N-2}{4}} \frac{\binom{N-4}{2}}{\binom{N-3}{3}} \frac{\binom{N-4}{2}}{\binom{N-4}{2}} \approx \frac{90}{N^2} , \tag{S25}$$

which is vanishingly small as $N \to \infty$ and therefore will not be observed in a typical 5-RR graph. These results are consistent with the negative-entropy regime at $\rho \gtrsim 0$ for $K = 5$, obtained by the mean-field cavity method (see Fig. S7), they also suggest the unlikely presence of cliques of size $n = 4$.

Applying the same analysis of Eq. (S25) to 3-RR and 4-RR graphs we find that the expected number of triangles is of order$O(1)$:

$$\binom{N}{3} \frac{\binom{N-3}{K-2}}{\binom{N-1}{K}} \frac{\binom{N-3}{K-2}}{\binom{N-2}{K-1}} \frac{\binom{N-3}{K-2}}{\binom{N-3}{K-2}} \approx \frac{K(K-1)^2}{6} , \tag{S26}$$

where $K = 3$ or $K = 4$. Therefore triangles will be observed in these graphs. These results are again consistent with the profile of $s(\rho)$ for the cases of $K = 3, 4$, which is always characterized by positive entropy, including those states with $\rho \sim 1/N$, i.e. states with small loops.

S5. STABILITY OF THE JACOBIAN MATRIX OF CAVITY PROBABILITIES

To examine the stability of the recursion relation of cavity probabilities around the BP fixed-point solution with fixed β, we examine the stability of the equation with respect to small perturbations $\delta q^{(c_1,c_2)}$, by considering the largest absolute eigenvalue of the corresponding Jacobian

matrix. We first differentiate Eq. (3) of the main text as follows:

$$\delta q^{0,0}_{j\to i} \equiv \delta q^{0,1}_{j\to i} = \frac{1}{z_{j\to i}} \sum_{l\in\partial j\setminus i} \Big[\prod_{k\in\partial j\setminus i,l} (q^{0,0}_{k\to j} + q^{1,0}_{k\to j}) \Big] (\delta q^{0,0}_{l\to j} + \delta q^{1,0}_{l\to j}) - \frac{1}{z^2_{j\to i}} \Big[\prod_{k\in\partial j\setminus i} (q^{0,0}_{k\to j} + q^{1,0}_{k\to j}) \Big] \delta z_{j\to i} \,, \tag{S27a}$$

$$\delta q^{1,0}_{j\to i} = \frac{e^{-\beta}}{z_{j\to i}} \sum_{l\in\partial j\setminus i} \Big[\sum_{\boldsymbol{c}_{\partial j\setminus i}} \Theta\Big(\sum_{k\in\partial j\setminus i} c_k - \frac{d_j}{2} \Big) \prod_{k\in\partial j\setminus i,l} q^{c_k,1}_{k\to j} \Big] \delta q^{c_l,1}_{l\to j} - \frac{1}{z^2_{j\to i}} \Big[\sum_{\boldsymbol{c}_{\partial j\setminus i}} \Theta\Big(\sum_{k\in\partial j\setminus i} c_k - \frac{d_j}{2} \Big) \prod_{k\in\partial j\setminus i} q^{c_k,1}_{k\to j} \Big] \delta z_{j\to i} \,, \tag{S27b}$$

$$\delta q^{1,1}_{j\to i} = \frac{e^{-\beta}}{z_{j\to i}} \sum_{l\in\partial j\setminus i} \Big[\sum_{\boldsymbol{c}_{\partial j\setminus i}} \Theta\Big(\sum_{k\in\partial j\setminus i} c_k + 1 - \frac{d_j}{2} \Big) \prod_{k\in\partial j\setminus i,l} q^{c_k,1}_{k\to j} \Big] \delta q^{c_l,1}_{l\to j} - \frac{1}{z^2_{j\to i}} \Big[\sum_{\boldsymbol{c}_{\partial j\setminus i}} \Theta\Big(\sum_{k\in\partial j\setminus i} c_k + 1 - \frac{d_j}{2} \Big) \prod_{k\in\partial j\setminus i} q^{c_k,1}_{k\to j} \Big] \delta z_{j\to i} \,, \tag{S27c}$$

where the change of normalization constant is

$$\begin{aligned} \delta z_{j\to i} = \sum_{l\in\partial j\setminus i} \Big\{ & 2 \Big[\prod_{k\in\partial j\setminus i,l} (q^{0,0}_{k\to j} + q^{1,0}_{k\to j}) \Big] (\delta q^{0,0}_{l\to j} + \delta q^{1,0}_{l\to j}) \\ & + e^{-\beta} \Big[\sum_{\boldsymbol{c}_{\partial j\setminus i}} \Theta\Big(\sum_{k\in\partial j\setminus i} c_k - \frac{d_j}{2} \Big) \prod_{k\in\partial j\setminus i,l} q^{c_k,1}_{k\to j} \Big] \delta q^{c_l,1}_{l\to j} \\ & + e^{-\beta} \Big[\sum_{\boldsymbol{c}_{\partial j\setminus i}} \Theta\Big(\sum_{k\in\partial j\setminus i} c_k + 1 - \frac{d_j}{2} \Big) \prod_{k\in\partial j\setminus i,l} q^{c_k,1}_{k\to j} \Big] \delta q^{c_l,1}_{l\to j} \Big\} \,. \end{aligned} \tag{S28}$$

We then re-write Eq. (S27) in terms of a, b, c and d given by Eq. (S11) to simplify the subsequent derivation, and assuming the uniformity of vertices in RR graphs:

$$\delta b_{j\to i} = \delta d_{j\to i} = \frac{1}{z} \sum_{l\in\partial j\setminus i} (D_{bc}\delta c_{l\to j} + D_{bb}\delta b_{l\to j}) - \frac{b}{z}\delta z \,, \tag{S29a}$$

$$\delta c_{j\to i} = \frac{e^{-\beta}}{z} \sum_{l\in\partial j\setminus i} (D_{ca}\delta a_{l\to j} + D_{cb}\delta b_{l\to j}) - \frac{c}{z}\delta z \,, \tag{S29b}$$

$$\delta a_{j\to i} = \frac{e^{-\beta}}{z} \sum_{l\in\partial j\setminus i} (D_{aa}\delta a_{l\to j} + D_{ab}\delta b_{l\to j}) - \frac{a}{z}\delta z \,, \tag{S29c}$$

where the coefficients are

$$D_{aa} = \sum_{r=\lceil \frac{K}{2}-1 \rceil -1}^{K-2} C_r^{K-2} a^r b^{K-r-2} \,, \tag{S30a}$$

$$D_{ab} = \sum_{r=\lceil \frac{K}{2}-1 \rceil}^{K-2} C_r^{K-2} a^r b^{K-r-2} \,, \tag{S30b}$$

$$D_{bb} = D_{bc} = (c+d)^{K-2} \,, \tag{S30c}$$

$$D_{ca} = \sum_{r=\lceil \frac{K}{2} \rceil -1}^{K-2} C_r^{K-2} a^r b^{K-r-2} \,, \tag{S30d}$$

$$D_{cb} = \sum_{r=\lceil \frac{K}{2} \rceil}^{K-2} C_r^{K-2} a^r b^{K-r-2} \,. \tag{S30e}$$

Since $a+b+c+d=1$ and $b=d$, we have $\delta a + \delta b + \delta c + \delta d = \delta a + 2\delta b + \delta c = 0$, and therefore we can write all the equations in terms of δa and δb only. We first re-write Eq. (S29a) as

$$\begin{aligned} \delta b_{j\to i} = \delta d_{j\to i} &= \frac{1}{z} \sum_{l\in \partial j \backslash i} D_{bb}(\delta b_{l\to j} + \delta c_{l\to j}) - \frac{b}{z}\delta z \\ &= \frac{1}{z} \sum_{l\in \partial j \backslash i} D_{bb}(-\delta a_{l\to j} - \delta b_{l\to j}) - \frac{b}{z}\delta z \,. \end{aligned} \tag{S31}$$

The variable δz is then given by the following equation in terms of δa and δb:

$$\delta z = \sum_{l\in \partial j \backslash i} \left[(e^{-\beta} D_{aa} - 2D_{bb} + e^{-\beta} D_{ca}) \delta a_{l\to j} + (e^{-\beta} D_{ab} - 2D_{bb} + e^{-\beta} D_{cb}) \delta b_{l\to j} \right] . \tag{S32}$$

Finally, we write down a 2×2 Jacobian matrix as

$$\mathcal{M} = \frac{1}{z} \begin{pmatrix} e^{-\beta} D_{aa} - a(e^{-\beta} D_{aa} - 2D_{bb} + e^{-\beta} D_{ca}) & e^{-\beta} D_{ab} - a(e^{-\beta} D_{ab} - 2D_{bb} + e^{-\beta} D_{cb}) \\ -D_{bb} - b(e^{-\beta} D_{aa} - 2D_{bb} + e^{-\beta} D_{ca}) & -D_{bb} - b(e^{-\beta} D_{ab} - 2D_{bb} + e^{-\beta} D_{cb}) \end{pmatrix} \tag{S33}$$

such that

$$\begin{pmatrix} \delta a_{j\to i} \\ \delta b_{j\to i} \end{pmatrix} = \sum_{l\in \partial j \backslash i} \mathcal{M} \begin{pmatrix} \delta a_{l\to j} \\ \delta b_{l\to j} \end{pmatrix} = (K-1)\mathcal{M} \begin{pmatrix} \delta a_{l\to j} \\ \delta b_{l\to j} \end{pmatrix} \,. \tag{S34}$$

Following the arguments in [5], when the largest absolute eigenvalue $|\lambda_{max}|$ of the Jacobian matrix $\mathcal{M}$ satisfies

$$(K-1)|\lambda_{max}| > 1 \,, \tag{S35}$$

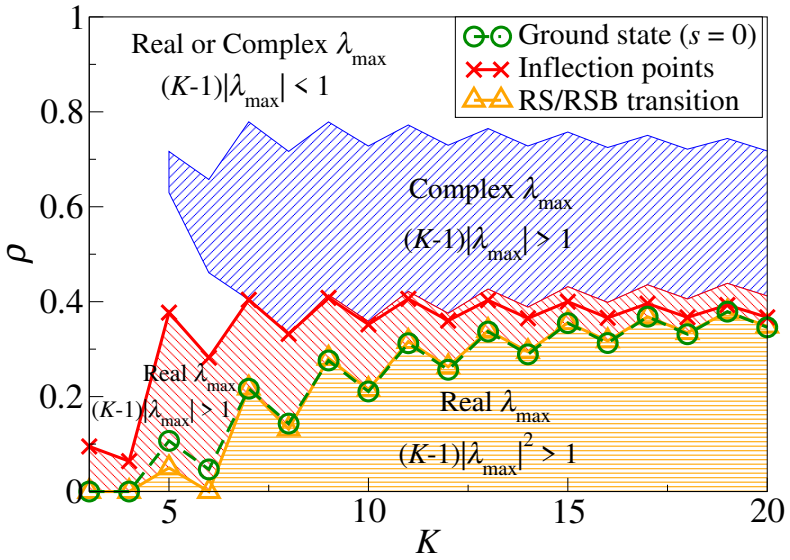

Figure S11: Comparing the value of the energy density ρ at the ground state (ρ_o determined by entropy density $s = 0$, circles), at the entropy inflection point (ρ_x, crosses), and at the RS/RSB (spin glass) transition point as determined by local stability analysis (triangles). The values of ρ which satisfy Eq. (S36), i.e. the RSB phase, are marked in orange (horizontal stripes); those which satisfy Eq. (S35) with real eigenvalues $\lambda_{\max}$, i.e. the modulation phase, are marked in red (stripes with negative slopes); and values that satisfy Eq. (S35) with complex eigenvalues $\lambda_{\max}$ are marked in blue (stripes with positive slopes).

the differences $(\delta a, \delta b)$ in the cavity probabilities diverge, which indicates the instability of the so-called liquid solution (the so-called modulation instability [5]).

On the other hand, when

$$(K-1)|\lambda_{max}|^2 > 1\ , \tag{S36}$$

the variances $(\langle(\delta a)^2\rangle, \langle(\delta b)^2\rangle)$ in the cavity probabilities diverge, which indicates the spin glass transition, i.e., the instability of a replica-symmetric (RS) solution to a replica-symmetry-breaking (RSB) solution.

As we can see in Fig. S11, the values of ρ of the RS/RSB spin-glass transition are consistent with (or just slightly above) the values of ρ_o at the ground state, except for $K = 5$ and 6. These results are obtained without computing the entropy of the system. They imply that the higher-free-energy branch ($\rho_o < \rho < \rho_x$) of the RS cavity theory is locally stable. In other words, the predicted discontinuous phase transition identified in the main text between the high-energy phase and the ground-state phase is not due to the emergence of the RSB behavior but an effect associated with

entropy inflection.

In addition, the values of ρ with a real $\lambda_{\max}$ satisfying Eq. (S35) (i.e. the red region) are generally found below the inflection points; specifically, these ρ values are consistent with the inflection points for $K = 3, \ldots, 6$. This implies that the inflection points roughly mark the onset of modulation instability, which may correspond to the fragmentation of the large alliances into smaller ones. This region is characterized by completely different SDA solutions, possibly with non-overlapping alliance members. On the other hand, we note that there is a large range of ρ above the inflection points where the eigenvalues $\lambda_{\max}$ are complex and $|\lambda_{\max}| > 1$ (i.e. the blue region). Nevertheless, since the eigenvalues are complex the instability on $(\delta a, \delta b)$ is rotational in nature, and neither cavity states a nor b vanish eventually. With an appropriate initial condition and a sufficiently slow adaptive iterative procedure, the iteration of the cavity equations lead to a uniform solution similar to the one found in the regime with $|\lambda_{\max}| < 1$. In this region, different SDA solutions with overlapping alliance members possibly co-exist, leading to uniform cavity probabilities a and b on individual nodes.

If the energy density ρ is kept fixed during the BP iterations, instead of the inverse temperature β, we find that the modulation instability disappears, and only the spin glass RS/RSB instability remains (at the β/ρ values identified before). For example, for the RR graph ensemble of degree $K = 12$, the ρ-fixed RS population dynamics simulations always converge to the uniform BP fixed-point determined by Eqs. (S9a)-(S9c), irrespective of the initial conditions, as long as $\rho \geq 0.263$. This stability threshold fully agrees with the theoretical prediction of the RS/RSB transition occurring at $\rho \approx 0.263$, which is only slightly above the predicted minimum energy density $\rho_o \approx 0.257$.

S6. THE POTENTIAL FOR A CLUSTERING TRANSITION

Besides the local stability analysis of Sec. S5, we also check the possibility of a spin glass dynamical (clustering) transition in the SDA problem. We follow the theoretical method of [6, 7] in this analysis. The corresponding first-step replica-symmetry-breaking (1RSB) results obtained by population dynamics simulations following Refs. [6, 7] reveal that the complexity of the system is identical to zero for $\rho > \rho_x$ (with ρ_x being the energy density of the inflection point), re-confirming that the discontinuous phase transition at $\rho > \rho_x$ as predicted by the mean field theory in the main text is not a spin glass transition but a phase transition resulting from the sigmoidal shape of the entropy function.

Here we list the most essential message-passing equations used in the 1RSB population dynamics. A systematic review of the 1RSB theory can be found in [4].

To investigate the possibility of an ergodicity-breaking transition at $\rho > \rho_x$, we consider the 1RSB mean field theory at $y = \beta$, where y is the inverse temperature at the level of macroscopic states. The distribution of the cavity probability function $q_{i\to j}$ among all macroscopic states is denoted as $Q_{i\to j}[q_{i\to j}]$. Let us first introduce an auxiliary probability functional

$$Q_{i\to j}^{c_i,c_j}[q_{i\to j}|\bar{q}_{i\to j}] \equiv \frac{Q_{i\to j}[q_{i\to j}]q_{i\to j}^{c_i,c_j}}{\bar{q}_{i\to j}^{c_i,c_j}} \ , \tag{S37}$$

where the mean cavity probability is defined as $\bar{q}_{i\to j} \equiv \int \mathcal{D}q_{i\to j}\ Q_{i\to j}[q_{i\to j}]q_{i\to j}$ (averaging over all the possible cavity probability functions). At $y = \beta$ the mean cavity probabilities $\bar{q}_{i\to j}$ on all the edges of the graph satisfy the BP equation [see Eq. (3) of the main text], and therefore they can be determined without knowing $Q_{i\to j}[q_{i\to j}]$. The functional $Q_{i\to j}^{c_i,c_j}[q_{i\to j}|\bar{q}_{i\to j}]$ can be understood as the conditional probability of drawing a cavity distribution $q_{i\to j}$ given the observed occupation states of vertex i being c_i and that of vertex j being c_j [6].

At $y = \beta$ the self-consistent equation for this auxiliary probability functional is derived to be

$$Q_{i\to j}^{c_i,c_j}[q_{i\to j}|\bar{q}_{i\to j}] = \sum_{\boldsymbol{c}_{\partial i\backslash j}} \Gamma_{i\to j}^{c_i,c_j}(\boldsymbol{c}_{\partial i\backslash j}) \prod_{k\in\partial i\backslash j} \int \mathcal{D}q_{k\to i} Q_{k\to i}^{c_k,c_i}[q_{k\to i}|\bar{q}_{k\to i}]\delta[q_{i\to j} - \hat{q}_{i\to j}] \ , \tag{S38}$$

where

$$\Gamma_{i\to j}^{c_i,c_j}(\boldsymbol{c}_{\partial i\backslash j}) \equiv \frac{\delta_{c_i}^0 \prod\limits_{k\in\partial i\backslash j} \bar{q}_{k\to i}^{c_k,0} + \delta_{c_i}^1 e^{-\beta}\Theta(\sum\limits_{k\in\partial i\backslash j} c_k + c_j - \frac{d_i}{2}) \prod\limits_{k\in\partial i\backslash j} \bar{q}_{k\to i}^{c_k,1}}{2\prod\limits_{k\in\partial i\backslash j}(\bar{q}_{k\to i}^{0,0} + \bar{q}_{k\to i}^{1,0}) + e^{-\beta}\sum\limits_{c_j}\sum\limits_{\boldsymbol{c}_{\partial i\backslash j}} \Theta(\sum\limits_{k\in\partial i\backslash j} c_k + c_j - \frac{d_i}{2}) \prod\limits_{k\in\partial i\backslash j} \bar{q}_{k\to i}^{c_k,1}} \ , \tag{S39}$$

and $\hat{q}_{i\to j}$ is a short-hand notation for the BP expression. The probability weights $\Gamma_{i\to j}^{c_i,c_j}(\boldsymbol{c}_{\partial i\backslash j})$ can be used to construct an occupation pattern $\boldsymbol{c}_{\partial i\backslash j} = \{c_k : k \in \partial i\backslash j\}$ for a focal vertex i, and then one can get a set of samples $q_{i\to j}$ following Eq. (S38) to represent $Q_{i\to j}^{c_i,c_j}[q_{i\to j}|\bar{q}_{i\to j}]$.

For the RR graph ensembles the 1RSB population dynamics simulations carried out for $\rho > \rho_x$ all evolve to the trivial fixed point of all the probability functionals $Q_{i\to j}^{c_i,c_j}[q_{i\to j}|\bar{q}_{i\to j}]$ and $Q_{i\to j}[q_{i\to j}]$ being Dirac's δ-functionals. This indicates that the system has only a single equilibrium macroscopic state at energy density $\rho > \rho_x$.

The same 1RSB analysis, based on population dynamics, may be carried out for $\rho < \rho_x$ to determine the precise value of the spin glass dynamical transition point; this is beyond the scope of the current study and will be the subject of future research.

S7. THE CLAMP-ALLIANCE (CA) ALGORITHM

Here we present the pseudo-code of the CA algorithm. Algorithm 1 is based on the modified BP message-passing protocol (see Sec. S3 B). The inverse temperature β is adjusted by solving Eq. (S20) after each BP iteration. The code of CA is accessible from the webpage `lib.itp.ac.cn/html/zhouhj/codes.htm`.

The performance of the CA algorithm is not sensitive to the precise value of objective density ρ. The CA results reported in Table I of the main text were obtained by setting the objective relative size $\rho = \rho_o$, with ρ_o being the estimated minimum energy density by the RS mean field theory. If the value of ρ_o is unknown, one can simply run the CA algorithm for a set of different objective ρ values and choose the minimum-size alliance set A obtained from these different trials.

For the alliance solutions A obtained by the CA algorithm for RR graphs, the subgraph induced by the vertices of each of these alliances forms only a single connected component.

Algorithm 1 Clamp-Alliance (CA) for the minimum strong defensive alliance problem. The output of CA is a vertex set (alliance) A such that each vertex $i \in A$ has at least one half of its nearest-neighbor vertices in A.

Input. A connected graph G of N vertices $i \in \{1, 2, \ldots, N\}$ and M edges (i, j) between pairs of vertices i and j.

Initialize. Set $S = \{1, 2, \ldots, N\}$; randomly assign cavity probability distributions $q_{i \to j}^{c_i, c_j}$ and $q_{j \to i}^{c_j, c_i}$ for all the edges (i, j); set decimation fraction η (e.g., $\eta = 0.005$); set objective relative size ρ of alliance; set iteration number t (e.g., $t = 10$) of belief-propagation.

while $S \neq \emptyset$ **do** ▷ reduce alliance size by BP-guided decimation

1. Set $A = S$.
2. Repeat t times the iteration of the modified BP equation [see Eqs. (S18) and (S21)] on all the edges between the vertices of S, adjusting the inverse temperature β of each BP iteration to satisfy condition (S20).
3. Compute the occupation probabilities q_i for all the vertices $i \in S$ according to $q_i = \frac{e^{-\beta} w_i^1}{\left(e^{-\beta} w_i^1 + w_i^0\right)}$ [see Eq. (S19)], and then rank these vertices in increasing order of q_i.
4. Delete the top fraction η of the vertices $i \in S$ (which have the smallest q_i values) from S.
5. Repeatedly delete a vertex $j \in S$ from S if j has less than $d_j/2$ nearest neighbors in S, until no more vertices need to be deleted.

end while

for every vertex $i \in A$ in a random order **do** ▷ refine the alliance

1. Set $S = A$.
2. Delete i from S.
3. Repeatedly delete a vertex $j \in S$ from S if j has less than $d_j/2$ nearest neighbors in S, until no more vertices need to be deleted.
4. If $S \neq \emptyset$, then set $A = S$.

end for

[1] S. Schnabel, D. T. Seaton, D. P. Landau, and M. Bachmann. Microcanonical entropy inlection points: Key to systematic understanding of transitions in finite systems. *Phys. Rev. E* **84**, 011127 (2011).

[2] E. Marinari and R. Monasson. Circuits in random graphs: from local trees to global loops. *J. Stat. Mech.: Theory Exper.*, P09004 (2004).

[3] Y. Kabashima and D. Saad. Statistical mechanics of error-correcting codes. *Europhys. Lett.* **45**, 97–103 (1999).

[4] M. M. Mézard and A. Montanari. *Information, Physics, and Computation.* Oxford University Press, Oxford, UK, 2009.

[5] O. Rivoire, G. Biroli, O. C. Martin, and M. Mézard. Glass models on bethe lattices. *Eur. Phys. J. B* **37**, 55–78 (2004).

[6] M. Mézard and A. Montanari. Reconstruction on trees and spin glass transition. *J. Stat. Phys.* **124**, 1317–1350 (2006).

[7] F. Krzakala, A. Montanari, F. Ricci-Tersenghi, G. Semerjian, and L. Zdeborová. Gibbs states and the set of solutions of random constraint satisfaction problems. *Proc. Natl. Acad. Sci. USA* **104**, 10318–10323 (2007).